Mixing in a drop moving through a serpentine channel: A computational study

Metin Muradoglu[a)]
Department of Mechanical Engineering, Koc University, Rumelifeneri Yolu, Sariyer 34450 Istanbul, Turkey

Howard A. Stone[b)]
Division of Engineering and Applied Sciences, Harvard University, Cambridge, Massachusetts 02139-4307

(Received 4 January 2005; accepted 31 May 2005; published online 20 July 2005)

The chaotic mixing in a drop moving through a winding channel is studied computationally in a two-dimensional setting. The molecular mixing is ignored and only the mixing due to the chaotic advection is considered. Passive tracer particles are used to visualize the mixing patterns and mixing is quantified by two distinct methods. It is found that both the quantification methods are consistent with visual observations as well as with each other. The effects of various non-dimensional parameters on the quality of mixing are studied and it is found that the capillary number, the ratio of the drop phase fluid viscosity to that of the ambient fluid and the relative size of the drop compared to the average channel width are the most critical parameters influencing the mixing. The mixing is found to be weakly dependent on Reynolds number. © *2005 American Institute of Physics*. [DOI: 10.1063/1.1992514]

I. INTRODUCTION

Rapid mixing is of essential importance in many microfluidic applications such as the homogenization of solutions of reagents used in chemical reactions, drug delivery, sequencing or synthesis of nucleic acids, protein crystallization, etc.[1–6] However, it is difficult to mix fluids in microchannels since flows in these channels are generally laminar and molecular diffusion is usually insufficient to mix fluids across the channel on the time scale of the usual residence time, especially in solutions containing macromolecules that have diffusion coefficients one or two orders of magnitude lower than that of ordinary small molecules.[6] To overcome this difficulty, the fluids must be manipulated to increase the interfacial surface area between initially distinct fluid regions and to reduce the striation length, which is characteristic of distinct chemical separation. The working principle of nearly all approaches for increasing mixing in small channels is essentially based on the concept of chaotic mixing.[6–9] The approach of chaotic mixing was first suggested in the early 1980s by Aref[10] as a way to produce efficient mixing in viscously dominated flows and has since been studied extensively.[9,11] One particular application that inspired the present study is the use of chaotic advection to enhance the mixing inside droplets in microchannels in order to perform kinetic measurements with high temporal resolution and low consumption of samples.[1,12,13]

The topic of chaotic mixing in a liquid droplet in a low-Reynolds number flow was first studied theoretically by Bajer and Moffat[14] and then by Stone *et al.*[15] and Kroujiline and Stone.[16] These studies make clear that the three-dimensional flow in a spherical droplet may exhibit chaotic streamlines in steady state conditions and other driving forces for fluid motion, either steady or unsteady, are capable of producing three-dimensional mixing flows inside a droplet.

The mixing in a droplet by chaotic advection has recently received significant attention and has been investigated experimentally by Song *et al.*[12,13] It has been shown that the reagents in a droplet (or plug) can be mixed rapidly as the liquid drop moves through a winding channel and the drop can be used as a chemical reactor to measure kinetics and binding constants of the reagents over millisecond time scales and also to measure the aspects of phase and reaction diagrams of multicomponent system. The use of drops as chemical reactors is very attractive due to lack of axial dispersion and low sample consumption. The experimental studies on the chaotic mixing inside drops moving through a winding channel have been reviewed by Bringer *et al.*[1] Stone and Stone[17] have recently extended the theoretical studies by considering time-periodic and nearly time-periodic flows inside a droplet to model the micro-mixer developed by Song *et al.*[13] Guenther *et al.*[2] have demonstrated experimentally that the mixing of the continuous phase can also be enhanced significantly by the motion of bubbles in a meandering channel. (See also Garstecki *et al.*[18]).

In this study, the chaotic mixing in a drop moving through a winding channel is studied computationally in a two-dimensional setting using a direct numerical simulation within the framework of a finite-volume(FV)/front-tracking(FT) method developed by Muradoglu.[18] The drop shape is calculated self-consistently, molecular mixing is ignored, and only the mixing by chaotic advection is considered. The mixing is visualized using passive tracer particles and is quantified using two different methods suggested by Krasnopolskaya *et al.*[20] and by Stone and Stone.[17]

In Sec. II we present a brief description of the math-

[a)]Author to whom correspondence should be addressed. Telephone: +90 (212) 338 14 73. Fax: +90 (212) 338 15 48. Electronic mail: mmuradoglu@ku.edu.tr
[b)]Telephone: +1 (617) 495 3599. Fax: +1 (617) 495 9837. Electronic mail: has@deas.harvard.edu

ematical formulation and computational method. The physical problem is discussed in Sec. III where the methods used for visualization and quantification of mixing are summarized. The results are presented and discussed in Sec. IV and some conclusions are drawn in Sec. V.

We note that this work complements the recent investigation of Stone and Stone[17] who used an analytical description of the three-dimensional flow inside a spherical drop to model the time-varying flows experienced by a drop in a serpentine channel. In this paper, we build on the study of Stone and Stone[17] as we solve the two-dimensional problem numerically, allow for drop deformation, and examine quantitatively the effect of capillary number, Reynolds number, drop size, and viscosity ratio.

II. FORMULATION AND NUMERICAL METHOD

The governing equations are described in this section in the framework of the front-tracking method in which the flow equations are written for the whole flow field, and different phases are treated with variable material properties.[21] The effects of surface tension are treated as body forces and added to the momentum equations as δ functions at the phase boundaries. In the Cartesian coordinates, the two-dimensional incompressible continuity and Navier–Stokes equations can be written in conservation form as

$$\frac{\partial \mathbf{q}}{\partial t}+\frac{\partial \mathbf{f}}{\partial x}+\frac{\partial \mathbf{g}}{\partial y}=\frac{\partial \mathbf{f}_v}{\partial x}+\frac{\partial \mathbf{g}_v}{\partial y}+\mathbf{f}_b, \tag{1}$$

where

$$\mathbf{q}=\begin{Bmatrix}0\\ \rho u\\ \rho v\end{Bmatrix}, \quad \mathbf{f}=\begin{Bmatrix}u\\ \rho u^2+p\\ \rho uv\end{Bmatrix}, \quad \mathbf{g}=\begin{Bmatrix}v\\ \rho uv\\ \rho v^2+p\end{Bmatrix}, \tag{2}$$

and

$$\mathbf{f}_v=\begin{Bmatrix}0\\ \tau_{xx}\\ \tau_{xy}\end{Bmatrix}, \quad \mathbf{g}_v=\begin{Bmatrix}0\\ \tau_{xy}\\ \tau_{yy}\end{Bmatrix}. \tag{3}$$

In Eqs. (1)–(3), x and y are the Cartesian coordinates and t is the physical time; ρ, μ and p are the fluid density, the dynamic viscosity and pressure, respectively, and u and v are the velocity components in x and y coordinate directions, respectively. The first row in Eq. (1) simply states that the velocity field is solenoidal while the last two rows represent the momentum conservation equations in x and y directions, respectively. The viscous stresses appearing in the viscous flux vectors are given by

$$\tau_{xx}=2\mu\frac{\partial u}{\partial x}, \quad \tau_{yy}=2\mu\frac{\partial v}{\partial y}, \quad \tau_{xy}=\mu\left(\frac{\partial u}{\partial y}+\frac{\partial v}{\partial x}\right). \tag{4}$$

The last term in Eq. (1) represents the body forces resulting from surface tension and is given by

$$\mathbf{f}_b=\int_S \sigma\kappa\mathbf{n}\delta(\mathbf{x}-\mathbf{x}^f)ds, \tag{5}$$

where $\delta, \mathbf{x}^f, \sigma, \kappa, \mathbf{n}, S$ and ds denote, respectively, the Dirac delta function, the location of the interface, the surface tension coefficient, twice the mean curvature, the outward unit normal vector on the interface, the surface area of the interface, and the surface area element of the interface.

In Eq. (1), it is assumed that the density of a fluid particle remains constant, i.e.,

$$\frac{D\rho}{Dt}=0, \tag{6}$$

where the substantial derivative is defined as $D/Dt=\partial/\partial t+\mathbf{u}\cdot\nabla$.

The governing equations [Eq. (1)] are solved by the finite-volume/front-tracking method developed by Muradoglu.[18] The method combines a finite-volume solver with the front-tracking method developed by Unverdi and Tryggvason.[21] The continuity and momentum equations are solved on a curvilinear grid using a finite-volume method. The spatial derivatives are approximated by a finite-volume method that is equivalent to second-order finite differences on a regular mesh. A dual (or pseudo) time-stepping method is employed to achieve time accuracy and an alternating direction implicit (ADI) method is used to perform integration in pseudo time. Fourth-order numerical dissipation terms are added to the discrete version of the flow equations to prevent the odd-even decoupling. Preconditioning, local time-stepping, and multigrid methods are used to accelerate the convergence rate of the ADI method in the pseudo time. Details of the FV method can be found in Refs. 22 and 18.

The interface boundary between the drop phase and the ambient fluid are represented by connected Lagrangian marker points moving with the local flow velocity interpolated from the neighboring curvilinear grid points. The communication between the curvilinear grid and the interface marker points is maintained efficiently using an auxiliary regular Cartesian grid cast on the curvilinear grid.[18] An indicator function is defined such that it is unity inside the droplet and zero outside. Based on the locations of the interface marker points, unit magnitude jumps are distributed in a conservative manner on the regular grid points near the interface and are integrated to compute the indicator function everywhere. This procedure involves solution of a Poisson equation on a regular grid and yields a smooth transition of the indicator function across the interface. The indicator function is then interpolated from the regular Cartesian grid onto the curvilinear grid using bilinear interpolations. Once the indicator function distribution is determined, the viscosity is set as a function of the indicator function. The interface marker points are also used to compute the surface tension forces at the interface which are then distributed on the neighboring curvilinear grid cells in a conservative manner and added to the discrete momentum equations as source terms. For the details of the FV/FT method, see Muradoglu[19] and Muradoglu and Gokaltun.[23]

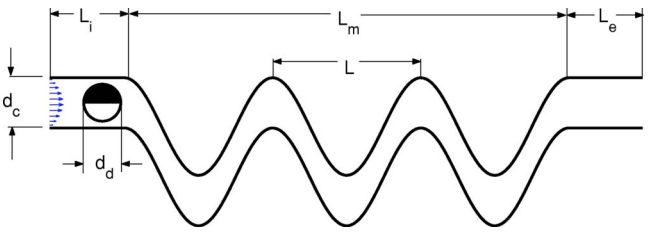

FIG. 1. The sketch of the channel used in the computations. The volume flow rate per unit width into the page is specified at the inlet based on a fully developed channel flow and the pressure is fixed at the exit. The flow is initialized as a single-phase steady flow using the ambient fluid properties and a cylindrical drop is then placed instantaneously in the ambient flow. The tracer particles are initially distributed uniformly in the drop at random and the particles filling the upper part of the drop are used for visualization.

Although the flow is incompressible in all the cases studied here, the drop volume changes due to accumulation of numerical errors especially when computations are performed on a coarse grid over a long time. To overcome these inevitable numerical errors, a correction algorithm is devised to maintain the drop volume constant within a prescribed error tolerance. The correction algorithm is essentially based on the procedure described by Cruchaga *et al.*[24] and it iteratively corrects the positions of the interface marker points until the global mass conservation in the drop is satisfied within the specified error tolerance. It is found that the correction algorithm is very robust and converges after a few iterations in all the cases presented in this paper. We note that, when the correction algorithm is switched off, the total change in drop volume is less than 10% in all the cases presented in this study. Since correction is performed in each time step and thousands of time steps are taken during a typical simulation, the error due to the correction is expected to be negligibly small.

III. PROBLEM STATEMENT AND QUANTIFICATION OF MIXING

A. Problem statement

The chaotic mixing inside a drop moving through a winding channel is studied in a two-dimensional setting. Although the flow is two-dimensional, it is time dependent and so time acts as a third dimension, which makes it possible for streamline patterns at one time to cross the streamline patterns at a later time and so produce effective mixing via chaotic trajectories. The channel consists of a straight entrance, a sinusoidal mixer and a straight exit section as sketched in Fig. 1. The lower and upper walls of the mixing section are defined by $y_l = a[1+\cos(2\pi x/L)]$ and $y_u = a[1+d_c/a+\cos(2\pi x/L)]$, respectively, so the channel maintains constant width. The parameters a, d_c, and L correspond to the scaling factor, the channel width at the inlet and the corrugation wavelength, respectively. The nondimensional parameter $\zeta = d_c/L$ is used to characterize the geometry. The smaller the values of ζ the weaker is the winding of the mixing section. The flow rate is specified at the inlet section assuming a fully developed velocity profile and a steady single-phase flow is computed first using the ambient fluid properties and is then used as the initial conditions. The average velocity at the inlet is denoted by U_i. The drop is instantaneously placed in the entrance section as sketched in Fig. 1 in an initially steady flow. The drop is initialized as a circle with diameter $d_d = 2R_d$. The properties of the drop phase and ambient fluid are denoted by subscripts "*d*" and "*o*," respectively. The governing nondimensional parameters are defined as the channel Reynolds number $Re = \rho_o U_i d_c/\mu_o$, the capillary number $Ca = \mu_o U_i/\sigma$, the viscosity ratio $\lambda = \mu_d/\mu_o$, the density ratio $\gamma = \rho_d/\rho_o$, and the ratio of the drop size to the channel inlet width $\Lambda = d_d/d_c$ where ρ_o and ρ_d are the ambient and drop phase fluid densities, and μ_o and μ_d are the ambient and fluid viscosities, respectively. Based on the inlet velocity and the corrugation wavelength, the nondimensional physical time is defined as $t^* = tU_i/L$.

Passive tracer particles are initially distributed uniformly at random within the drop and the particles occupying the lower half of the drop are identified as "white" while the other particles are "black."[25] These particles are moved with the local flow velocity interpolated from the neighboring computational grid points using the same advection scheme as used for moving the interface marker points.

Finally, we complete the specification of the geometry by fixing L_i, the length of the inlet portion of the channel, L_e, the length of the exit portion of the channel, and L_m, the length of the mixing portion of the channel as sketched in Fig. 1.

B. Quantification of mixing

The tracer particles are used to visualize the mixing patterns inside the drop and two distinct methods are used to quantify the quality of mixing. The first method developed by Stone and Stone[17] measures the quality of mixing in terms of the "mixing number" defined as follows: Let tracer particles $1,\ldots,N$ have locations $\mathbf{x}_i$, and let $Opp(\mathbf{x}_i)$ be the set of locations of all tracer particles of color opposite to the color of the particle located at $\mathbf{x}_i$. Also, let $d(\mathbf{x}_i,\mathbf{x}_j)$ denote the Cartesian distance from particle i to particle j, S be a set of tracer particles, and define $d(\mathbf{x}_i,S) \equiv \min_j\{d(\mathbf{x}_i,s_j)\}$, where $s_j \in S$ and $\min_j$ indicates a minimum taken over all s_j. Then the mixing number $m(t)$ for the drop is defined as

$$m(t) = \sum_{i=1}^{N} \frac{d^2[x_i, Opp(\mathbf{x}_i)]}{N}. \tag{7}$$

In all the results presented here, the mixing number is scaled by the initial ($t=0$) value of mixing number. The mixing number is attractive since it is easy to compute and more importantly it is grid independent.[17] However, it does not completely characterize the structure of the mixing patterns. We also use the measures suggested by Krasnopolskaya *et al.*[20] In this method, the drop area S_d is divided into N_δ square pixels of width size δ for a side and with an area of $S_\delta = \delta^2$ so that the drop area can be written approximately as $S \cong N_\delta S_\delta$. Then a coarse-grained probability density function is defined as $D_n = N_b^{(n)}/(N_b^{(n)}+N_w^{(n)})$, where $N_b^{(n)}$ and $N_w^{(n)}$ are the number of "black" and "white" tracer particles in the nth pixel, respectively. The probability density function (PDF) is then defined as

$$\langle D\rangle = \frac{1}{N_\delta}\sum_{\delta n=1}^{N_\delta} D_n = \frac{N_\delta}{N_b + N_w}, \tag{8}$$

where N_b and N_w are the total number of the "black" and "white" particles, respectively. Note that the PDF remains constant in the course of mixing so that it can be used as a measure for the accuracy of the numerical computations. On the other hand, the average of the square density, $\langle D_n^2\rangle$, results in the following inequality:

$$\langle D^2\rangle = \frac{1}{N_\delta}\sum_{\delta n=1}^{N_\delta} D_n^2 < \frac{N_b}{N_b + N_w}, \tag{9}$$

since $D_n \leqslant 1$ and cannot be unity in all of the pixels unless all the tracer particles have the same color. Based on the coarse-grained density, the entropy of the mixtures is defined as

$$s = -\langle D \log D\rangle = -\frac{1}{N_\delta}\sum_{\delta n=1}^{N_\delta} D_n \log D_n. \tag{10}$$

The entropy is always positive since $0 < D < 1$ and grows in time to its maximum

$$s_o = -\lim_{t\to\infty}\langle D \log D\rangle = -\langle D\rangle \log\langle D\rangle, \tag{11}$$

when the fluids in the drop are fully mixed. In all the results presented in this study, the entropy is normalized by s_o. Finally, the intensity of segregation is defined as

$$I = \frac{\langle (D - \langle D\rangle)^2\rangle}{\langle D\rangle(1 - \langle D\rangle)}. \tag{12}$$

In the case of complete mixing, the intensity of segregation tends to zero since the quantity $\langle (D - \langle D\rangle)^2\rangle$ tends to zero. The quality of mixing denoted by Q can be defined as the inverse of the intensity of segregation, i.e., $Q = 1/I$. In the present study, we prefer to use the intensity of segregation rather than the mixing quality since it varies between zero and unity.

As mentioned above, the PDF is a good measure for the accuracy of computations while the entropy and intensity are very useful measures for the quality of the internal mixing since they both account not only for the local structure of the mixing but also for the overall mixing patterns. However, both the entropy and intensity are strongly dependent on the pixel size and the number of tracer particles in each pixel. Therefore the mixing number, PDF, entropy and intensity measures are used together to quantify the quality of mixing.

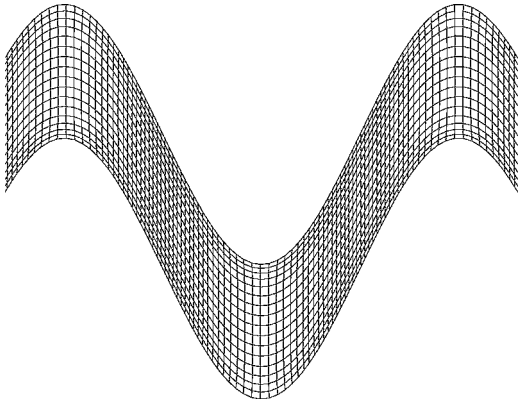

FIG. 2. A portion of a typical (coarse) curvilinear grid containing 256 $\times$16 cells. Finer versions of this grid, i.e., with 1024$\times$64 grid cells, are used in the computations.

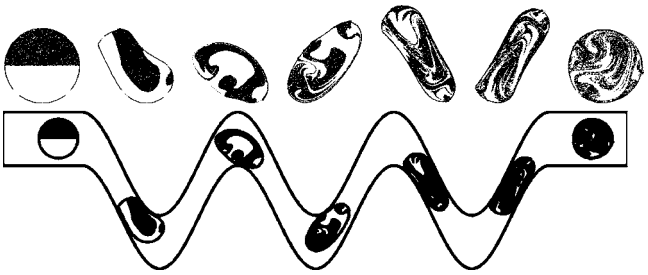

FIG. 3. Snapshots of mixing patterns taken at the nondimensional times from left to right t^*=0, 0.42, 0.90, 2.32, 1.80, 2.22 and 2.64, respectively. The top plots are the enlarged versions of the corresponding scatter plots shown in the channel (bottom plots). (Ca=0.025, Re=6.6, λ=1.0, Λ=0.76, Grid: 1024$\times$64.)

IV. RESULTS AND DISCUSSION

The computational results for the mixing by chaotic advection within a two-dimensional drop moving through a winding channel are presented in this section. A portion of a typical curvilinear (coarse) grid with 256$\times$16 cells is plotted in Fig. 2 to show the overall structure of the grid used in the computations. Unless stated otherwise, a 1024$\times$64 grid is used in all of the computations presented in this paper. The geometric parameter is set to ζ=0.33 and the density ratio is kept constant at unity in all of the computations reported here since density has no significant effect in low-Reynolds-number flows. First the evolution of the mixing patterns in the drop moving through the winding channel is presented. Then the effects of the nondimensional parameters such as the capillary number (Ca), the relative drop radius (Λ), the viscosity ratio (λ) and, the Reynolds number (Re) are studied. Scatter plots of the tracer particles are used to visualize the mixing patterns and only the "black" particles that initially occupy the upper half of the drop are used for visual clarity in all of the scatter plots presented. The particles escaping from the drop interface due to numerical error are disregarded. We emphasize that the total number of particles escaping from the drop interface between the inlet and the exit sections of the channel is less than 3% in all of the results presented. In computing the intensity of segregation, PDF and entropy, the total number of tracer particles is initially set to 40 000 and the pixel size is determined such that there are about 10 particles in each pixel.

In Fig. 3, snapshots of the tracer particle distributions,

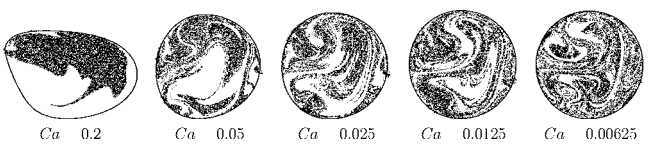

FIG. 4. The mixing patterns at the exit of the channel. (Re=6.6, λ=1.0, Λ=0.76, Grid: 1024$\times$64.)

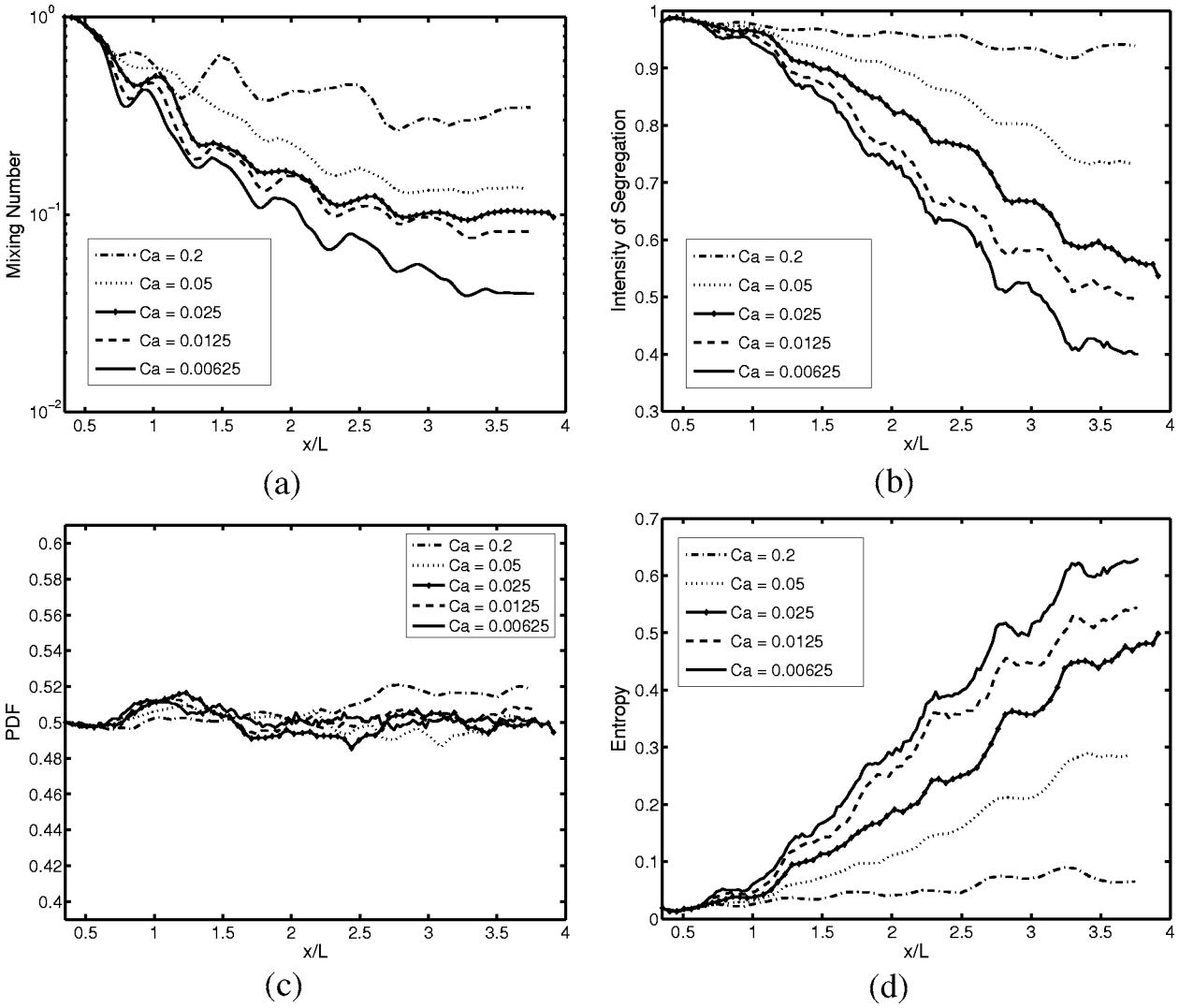

FIG. 5. Effect of the capillary number on mixing. (a) Mixing number, (b) intensity of segregation, (c) PDF, (d) entropy. ($Re=6.6, \lambda=1.0, \Lambda=0.76$, Grid: 1024×64.)

taken at the nondimensional times $t^*=0$, 0.42, 0.9, 1.32, 1.8, 2.22 and 2.64, are plotted to demonstrate the evolution of the mixing patterns in the drop while it moves through the model winding channel. The nondimensional parameters are $Ca=0.025$, $Re=6.6$, $\Lambda=0.76$, and $\lambda=1.0$. This case is taken as the base case and the effects of the nondimensional parameters are examined by systematically varying them one at a time. Note that typical values used in experiments[13] are $\rho_o \simeq 1.6\times10^3$ kg/m^3, $\rho_i \simeq 10^3$ kg/m^3, $\mu_o \simeq 5.1\times10^{-3}$ N·s/m^2, $\mu_i \simeq 10^{-3}$ N·s/m^2, $U_i \simeq 0.19$ m/s, $d_c \simeq 5.0\times10^{-5}$ m, and $\sigma \simeq 0.013$ N/m, which yields a Reynolds number approximately $Re \simeq 3$, a capillary number $Ca \simeq 0.07$ and a viscosity ratio $\lambda \simeq 0.2$. The mixing patterns are enlarged in the top plots given in Fig. 3 to better show the details of the mixing process. As can be clearly seen in this

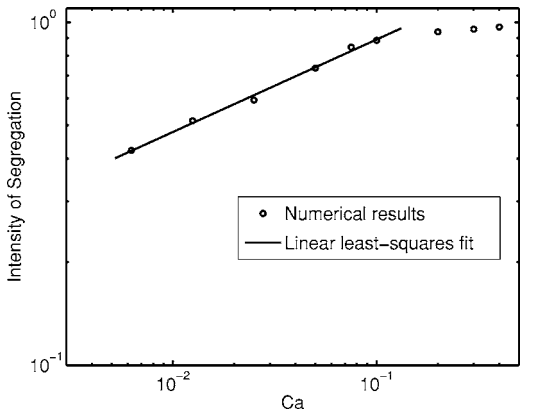

FIG. 6. The intensity of segregation against the capillary number at the time when the nondimensional component of drop centroid, $x/L=3.5$. The solid line is linear least-squares fit to the numerical data. The linear-least squares fit shows that the intensity of segregation asymptotically scales as $I \simeq 1.66Ca^{0.27}$ when $Ca \leqslant 0.1$. ($Re=6.6, \lambda=1.0, \Lambda=0.76$, Grid: 1024×64.)

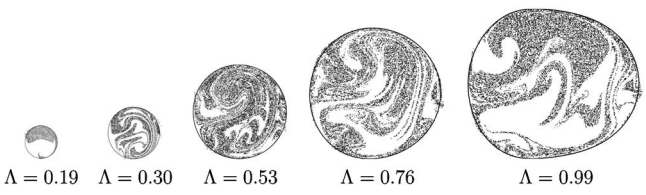

FIG. 7. The mixing patterns at the exit of the channel for nondimensional drop sizes $\Lambda=0.19$, 0.30, 0.53, 0.76 and 0.99 from left to right, respectively. ($Re=6.6, Ca=0.025, \lambda=1.0$, Grid: 1024×80 for $\Lambda=0.19$, 0.3 and 0.53, and 1024×64 for the others.)

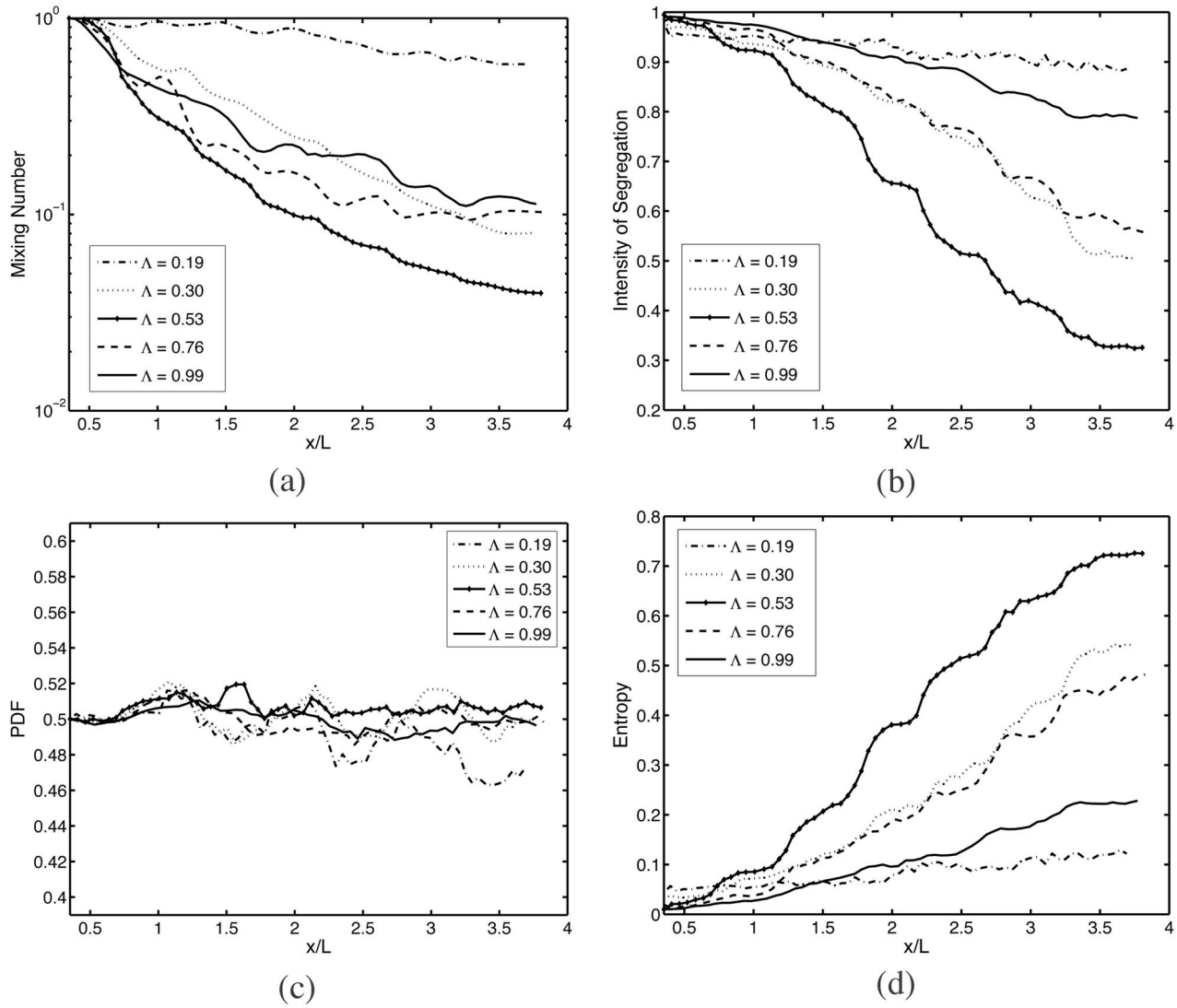

FIG. 8. Effect of drop size on mixing. (a) Mixing number, (b) intensity of segregation, (c) PDF, (d) entropy. ($Ca=0.025, Re=6.6, \lambda=1.0$.)

figure, chaotic advection occurs in a drop as it moves through a winding channel and the mixing patterns qualitatively resemble the actual three-dimensional mixing patterns.[13]

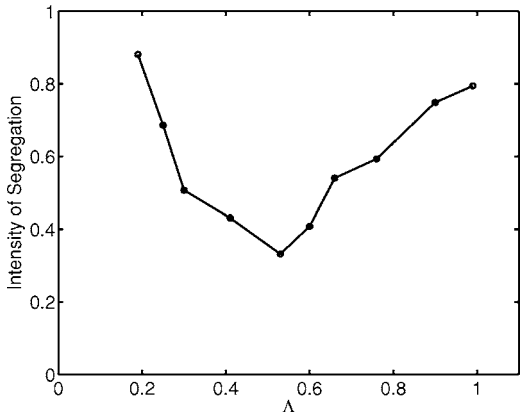

FIG. 9. The intensity of segregation against the relative drop size at the time when the nondimensional component of drop centroid, $x/L=3.5$. The plot shows that the best mixing occurs approximately for $\Lambda \simeq 0.5$. ($Ca=0.025, Re=6.6, \Lambda=0.76$, Grid: 1024×64.)

We next study the effects of the capillary number on the mixing patterns. For this purpose, the mixing patterns at the exit of the channel are plotted in Fig. 4 for capillary numbers $Ca=0.2$, 0.05, 0.025, 0.0125 and 0.00625. Note that the other parameters are kept constant at the base values. As can be seen in this figure, the mixing is increased dramatically as the capillary number is decreased and the drop is closer to a circular shape. The effects of the capillary number are quantified in Fig. 5 where the mixing number, the intensity of segregation, PDF and entropy are plotted as a function of the nondimensional component of the drop centroid, x/L. As can be seen in this figure, the mixing is very poor for $Ca=0.2$ and increases rapidly as Ca decreases. It is also observed in

FIG. 10. The mixing patterns at the exit of the channel as a function of the viscosity ratio. ($Ca=0.025, Re=6.6, \Lambda=0.76$, Grid: 1024×64.)

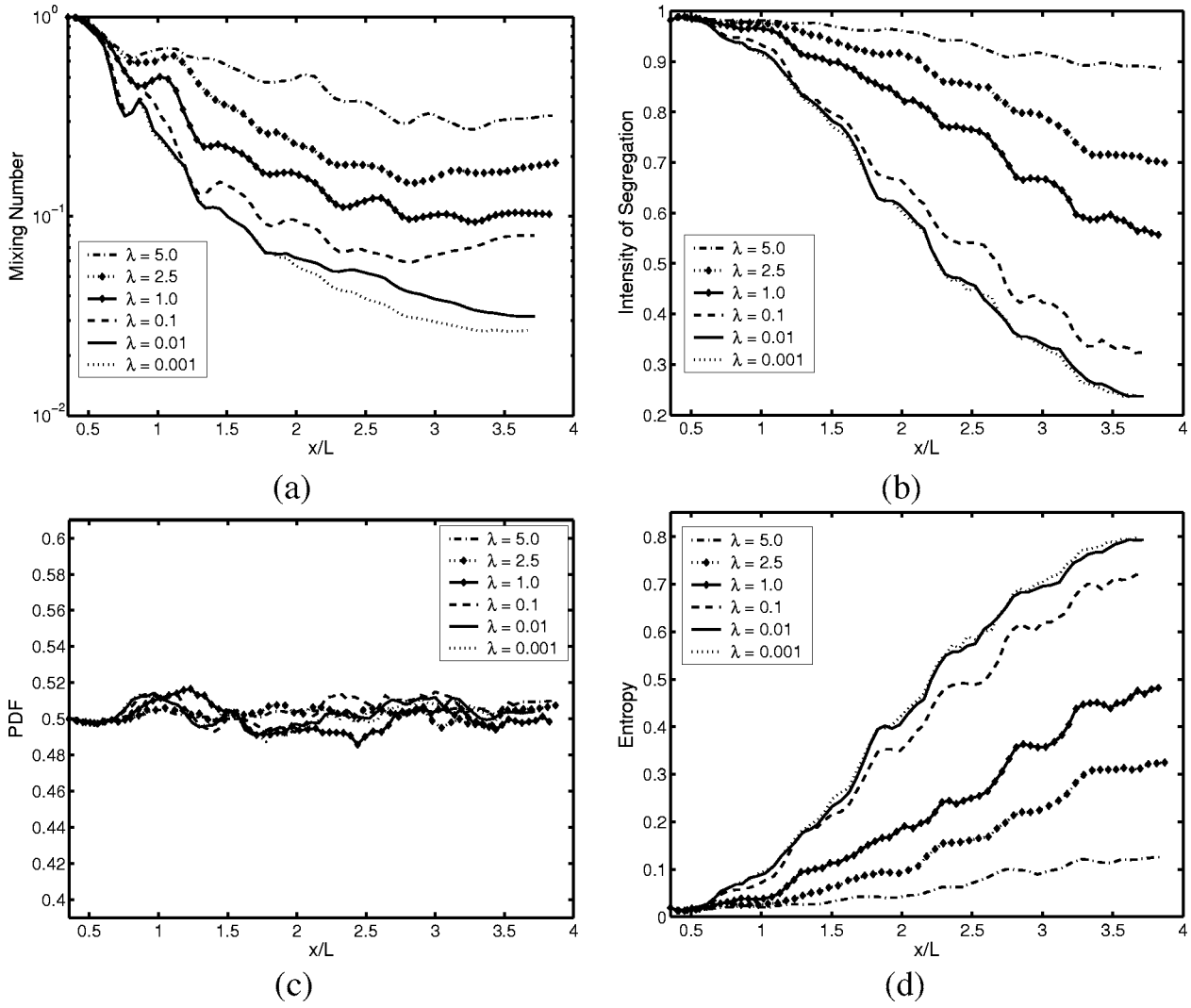

FIG. 11. Effect of viscosity ratio on mixing. (a) Mixing number, (b) intensity of segregation, (c) PDF, (d) entropy. ($Ca=0.025, Re=6.6, \Lambda=0.76$, Grid: 1024×64.)

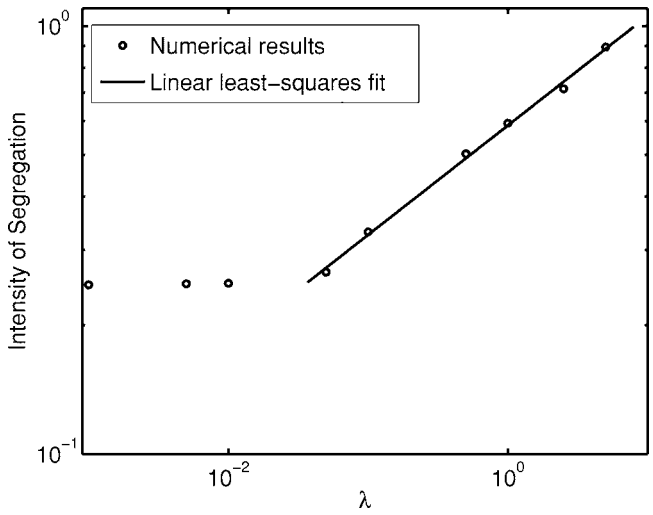

FIG. 12. The intensity of segregation against the viscosity ratio at the time when the nondimensional component of drop centroid, $x/L=3.5$. The solid line is linear least-squares fit to the numerical data. The linear-least squares fit shows that the intensity of segregation asymptotically scales as $I \simeq 0.6\lambda^{0.26}$ when $\lambda > 0.05$. ($Ca=0.025, Re=6.6, \Lambda=0.76$, Grid: 1024×64.)

Fig. 5 that each of the scalar measures, i.e., the mixing number, the intensity of segregation and the entropy are consistent in representing the quality of mixing and a nearly constant value of PDF indicates the accuracy of the computational results. The intensity of segregation is plotted against Ca in Fig. 6 at the time when the nondimensional component of drop centroid, $x/L=3.5$. The figure shows that the intensity of segregation approximately scales as $I \simeq 1.66Ca^{0.27}$ when $Ca \leqslant 0.1$ and it remains roughly constant at $I \simeq 0.9$ if $Ca > 0.1$. We do not have a quantitative expla-

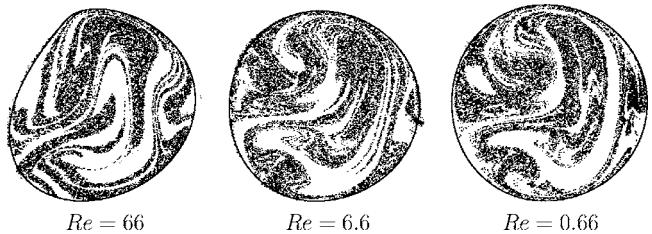

FIG. 13. The mixing patterns at the exit of the channel as a function of the Reynolds number. ($Ca=0.025, \lambda=1.0, \Lambda=0.76$, Grid: 1024×64.)

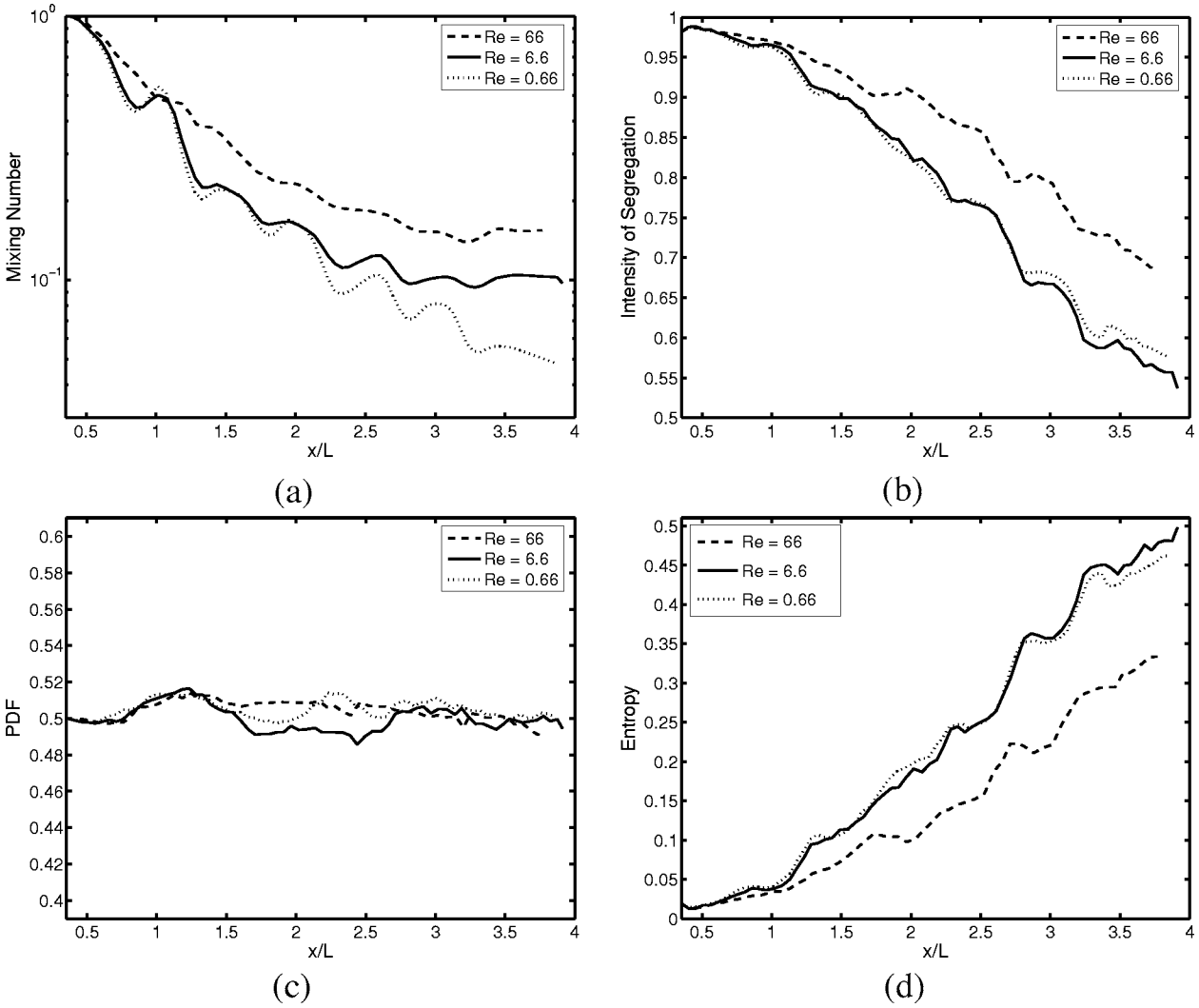

FIG. 14. Effect of the Reynolds number on mixing. (a) Mixing number, (b) intensity of segregation, (c) PDF, (d) entropy. ($Ca=0.025, Re=6.6, \lambda=1.0, \Lambda=0.76$, Grid: 1024×64.)

nation for this power-law scaling though it shows the strong influence of drop deformability on the internal mixing.

It has been observed experimentally that the best mixing occurs when the drop size is comparable to the channel width, see for instance, Song *et al.*[13] and Bringer *et al.*[1] This feature is verified in the numerical results presented in Figs. 7 and 8. Note that the channel width at the entrance for the model winding channel used in this study is larger than the average channel width and the average channel width in the mixing section is roughly half of the entrance width so a drop diameter equal to the mixing section of the channel is $\Lambda=0.5$. In Fig. 7, the mixing patterns are shown in the exit section of the channel for the nondimensional drop sizes of $\Lambda=0.19$, 0.30, 0.53, 0.76 and 0.99. The effects of the drop size on the quality of mixing are quantified in Fig. 8 where the mixing number, intensity of segregation, PDF and entropy are plotted against the nondimensional coordinate x/L of the drop centroid. As can be seen, the drop size has a strong effect on the mixing and the best mixing is obtained when the drop size is comparable to the channel width. To better show the effects of the drop size, the intensity of segregation is plotted as a function of the nondimensional drop size in Fig. 9 at the time when the nondimensional component of drop centroid, $x/L=3.5$. It is clear from these results that among the 10 cases studied the best mixing occurs for $\Lambda=0.53$.

The effects of the viscosity ratio on the mixing are shown in Figs. 10 and 11. In Fig. 10, the mixing patterns at the exit of the channel are plotted for the viscosity ratios $\lambda=0.01$, 0.1, 1.0, 2.5 and 5.0. As can be seen, the fluid inside the drop is almost fully mixed in the case of $\lambda=0.01$ while the mixing is very poor when $\lambda=5.0$. The results are further quantified in Fig. 11. Mixing is increased dramatically when the viscosity of the drop phase is decreased compared to the ambient fluid viscosity but the increase in mixing slows down when the viscosity ratio is smaller than $\lambda=0.1$. On the other hand, mixing is decreased rapidly in the case that the viscosity of the drop phase is larger than the ambient fluid viscosity and there is only weak, slow mixing after the viscosity ratio is larger than 5. To better quantify the effects of the viscosity ratio on the quality of mixing, the intensity of segregation is plotted against the viscosity ratio in Fig. 12 at

the time when the nondimensional component of drop centroid, $x/L=3.5$. As can be seen in this figure, for the mixing length used in the simulations, the intensity of segregation approximately scales as $I \simeq 0.6\lambda^{0.26}$ when $\lambda \geqslant 0.05$ (recall $I \leqslant 1$ by definition) and remains roughly constant at $I \simeq 0.27$ when $\lambda < 0.05$.

Finally, the effects of the Reynolds number on the mixing are shown in Figs. 13 and 14. In Fig. 13, it is seen qualitatively that the effects of the Reynolds number on the mixing patterns are not dramatic but the mixing is better for the lower Reynolds numbers. The quantitative results in Fig. 14 illustrate that mixing is only weakly dependent on the Reynold number when *Re* is of order of unity or smaller. Although not shown here, we note that flow separation occurs in the bending sections of the channel for $Re=66$.

V. CONCLUSIONS

The chaotic mixing in a drop moving through a winding, or serpentine, channel is studied computationally using the FV/FT method.[18] Tracer particles are used to visualize the mixing patterns and two distinct methods are employed for quantifying the quality of mixing. All of the mixing measures are found to be consistent with each other as well as with the visual evaluations of mixing for all the cases presented. It is observed that a chaotic mixing occurs inside a two-dimensional drop as it moves through a winding channel and the mixing patterns resemble the experimentally observed three-dimensional mixing patterns. Therefore we studied the mixing in a two-dimensional setting and examined the effects of the various nondimensional parameters on mixing. We found that the best mixing is obtained when the drop size is comparable with the channel width. The capillary number strongly influences the mixing process and the smaller the capillary number, corresponding to smaller drop deformation, the better is the mixing. We observed that the viscosity ratio of the drop phase and the ambient fluid also has a strong influence on the quality of mixing. The smaller the viscosity of the drop phase fluid compared to the viscosity of the ambient fluid, the better the quality of mixing. We also found that there is a threshold value of the viscosity ratio below which the influence of the viscosity ratio decreases rapidly. Finally, we observed that the Reynolds number has no significant influence on the mixing but the smaller the Reynolds number, the better the quality of mixing.

ACKNOWLEDGMENTS

The first author (M.M.) gratefully acknowledges the Harvard University–Koc University exchange scholar program for the financial support during his visit to Harvard University where the present work was started. H.A.S. is grateful to Unilever Research for research support. We thank Z. B. Stone for helpful conversations.

[1] M. R. Bringer, C. J. Gerdts, H. Song, J. D. Tice, and R. F. Ismagilov, "Microfluidic systems for chemical kinetics that rely on chaotic mixing in droplets," Philos. Trans. R. Soc. London, Ser. A **362**, 1087 (2004).
[2] A. Guenther, S. A. Khan, M. Thalmann, F. Trachsel, and K. F. Jensen, "Transport and reaction in microscale segmented gas-liquid flow," Lab Chip **4**, 278 (2004).
[3] J. Knight, "Honey, I shrank the lab," Nature (London) **418**, 474 (2002).
[4] K. F. Jensen, "Micromechanical systems: Status, challenges and opportunities," AIChE J. **45**, 2051 (1999).
[5] R. F. Service, "Minaturization puts chemical plants where you want them," Science **282**, 400 (1998).
[6] H. A. Stone, A. D. Stroock, and A. Ajdari, "Engineering flows in small devices: Microfluidics toward a lab-on-a-chip," Annu. Rev. Fluid Mech. **36**, 381 (2004).
[7] R. H. Liu, M. A. Stremler, K. V. Sharp, M. G. Olsen, J. G. Santiago, R. J. Adrian, H. Aref, and D. J. Beebe, "Passive mixing in a three-dimensional serpentine microchannel," J. Microelectromech. Syst. **9**, 190 (2000).
[8] A. D. Stroock, S. K. W. Dertinger, A. Ajdari, I. Mezic, H. A. Stone, and G. M. Whitesides, "Chaotic mixer for microchannels," Science **295**, 647 (2002).
[9] S. Wiggins and J. M. Ottino, "Foundations of chaotic mixing," Philos. Trans. R. Soc. London, Ser. A **362**, 1087 (2004).
[10] H. Aref, "Stirring by chaotic advection," J. Fluid Mech. **143**, 1 (1984).
[11] J. M. Ottino, *The Kinematics of Mixing* (Cambridge University Press, Cambridge, 1989).
[12] H. Song, M. R. Bringer, J. D. Tice, C. J. Gerdts, and R. F. Ismagilov, "Scaling of mixing by chaotic advection in droplets moving through microfluidic channels," Appl. Phys. Lett. **83**, 4662 (2003).
[13] H. Song, J. D. Tice, and R. F. Ismagilov, "A microfluidic system for controlling reaction networks in time," Angew. Chem., Int. Ed. **42**, 768 (2003).
[14] K. Bajer and H. K. Moffat, "On a class of steady confined Stokes flows with chaotic streamlines," J. Fluid Mech. **212**, 337 (1990).
[15] H. A. Stone, A. Nadim, and S. H. Strogatz, "Chaotic streamline inside drops immersed in steady Stokes flows," J. Fluid Mech. **232**, 629 (1991).
[16] D. Kroujiline and H. A. Stone, "Chaotic streamlines in steady bounded three-dimensional Stokes flows," Physica D **130**, 105 (1999).
[17] Z. B. Stone and H. A. Stone, "Imaging and quantifying mixing in a model droplet micromixer," Phys. Fluids **17**, 063103 (2005).
[18] P. Garstecki, M. A. Fischbach, and G. M. Whitesides, "Design for mixing using bubbles in branched microfluidic channels" Appl. Phys. Lett. **86**, 244108 (2005).
[19] M. Muradoglu, "A finite-volume/front-tracking method for computations of multiphase flows in complex geometries," in *Frontiers of Computational Fluid Dynamics 2006*, edited by D. A. Caughey and M. M. Hafez (World Scientific, Singapore, in press).
[20] T. S. Krasnopolskaya, V. V. Meleshko, G. W. M. Peters, and H. E. M. Meijer, "Mixing in Stokes flow in an annular wedge cavity," Eur. J. Mech. B/Fluids **18**, 793 (1999).
[21] S. O. Unverdi and G. Tryggvason, "A front-tracking method for viscous, incompressible flows," J. Comput. Phys. **100**, 25 (1992).
[22] D. A. Caughey, "Implicit multigrid computation of unsteady flows past cylinders of square cross-section," Comput. Fluids **30**, 940 (2001).
[23] M. Muradoglu and S. Gokaltun, "Implicit multigrid computations of buoyant drops through sinusoidal constrictions," ASME J. Appl. Mech. **71**, 1 (2004).
[24] M. Cruchaga, D. Celentano, and T. E. Tezduyar, "A moving Lagrangian interface technique for flow computations over fixed meshes," Comput. Methods Appl. Mech. Eng. **191**, 525 (2001).
[25] Because of the expense of printing color images we display all figures as black and white in the present paper. The readers interested in color images can contact the authors.